Extremely Weak Cold-Air Mass Flux and Extratropical Direct Meridional Circulation Linked to the Record-Warm Winter 2019/2020 over East Asia

Chiaki Kobayashi[1], Shuhei Maeda[2], Yuki Kanno[3], and Toshiki Iwasaki[4]
[1]*Meteorological Research Institute*, *Tsukuba*, *Japan*
[2]*Japan Meteorological Agency*, *Tokyo*, *Japan*
[3]*Central Research Institute of Electric Power Industry*, *Abiko*, *Japan*
[4]*Graduate School of Science*, *Tohoku University*, *Sendai, Japan*

Abstract

We examine the relationship between the record-warm winter (DJF) 2019/2020 over East Asia and the extremely weak hemispheric circulation anomaly. During this period, the polar cold-air mass (PCAM) flux over East Asia was the weakest on record since the DJF 1958/1959 due to the weak Siberian High. The zonal averaged surface temperature over the Northern Hemisphere mid-latitudes in DJF 2019/2020 was the highest since DJF 1958/1959 and was linked to the weakest PCAM flux at the mid-latitudes. The zonal mean field during this period was characterized by weak stationary waves, weak wave activity as diagnosed by Eliassen-Palm flux, and, to balance with this, record-weak extratropical direct meridional circulation (EDC). The weak EDC corresponded to weaker-than-normal meridional heat exchange and was consistent with warm anomalies in the Northern Hemisphere mid-latitudes, since the lower branch of EDC corresponds to zonally averaged cold air outflow. In addition, the statistical relationship also indicates the EDC intensity is negatively correlated with the surface temperature anomaly over East Asia.

(**Citation**: Kobayashi, C., S. Maeda, Y. Kanno, and T. Iwasaki, 2022: Extremely weak cold-air mass flux and extratropical direct meridional circulation linked to the record-warm winter 2019/2020 over East Asia. *SOLA*, **18**, 1−7, doi:10.2151/sola.2022-001.)

1. Introduction

The seasonal mean surface temperatures in winter 2019/2020 (December 2019 to February 2020; hereafter DJF 2019/2020) in Japan were the highest since DJF 1897/1898 (JMA 2020); the extreme warm weather was attributed to the persistent northward meandering of the subtropical jet stream over and around Japan (JMA 2020). Regarding the warm winter 2019/2020 in the Northern Hemisphere (NH), Lawrence et al. (2020) indicated strong stratospheric polar vortex condition and unusually weak wave activity from the troposphere. They discussed the link between the stratospheric polar vortex and Arctic Oscillation (AO) pattern enhancements as a two-way coupling between the troposphere and stratosphere. Regarding the warm winter in East Asia, the influence of tropical sea-surface temperature (SST) anomalies across the central Pacific and Indian Oceans during this period has been indicated. Doi et al. (2020) indicated that active convective activity over the western pole of the Indian ocean dipole caused the warm winter in East Asia. Kuramochi et al. (2021) suggested that the propagation of Rossby waves due to active convection over the western Indian Ocean may have formed anticyclonic circulation anomalies over East Asia, thereby contributing to the warm winter in East Asia.

Winter climate in East Asia is strongly affected by cold-air outbreaks transfering polar cold-air mass (PCAM) southward, i.e., from high- to mid-latitudes. As indicated by Iwasaki et al. (2014), climatological PCAM is discharged in the mid-latitudes along two main streams: the East Asian and North American streams. Iwasaki et al. (2014) also explained that angular momentum is transferred from the cold-air streams to the upward Eliassen-Palm (EP) flux in the exit regions of these PCAM streams; the extratropical direct meridional circulation (EDC) is generated via wave–mean-flow interactions. Therefore, the interannual variability of PCAM streams over East Asia is considered to be related to NH circulation variability through the EDC.

In this study, we perform isentropic PCAM analysis (Iwasaki et al. 2014) and mass-weighted isentropic zonal-mean (MIM) analysis (Iwasaki 1989, 1992) to describe the atmospheric state of DJF 2019/2020. The hemispheric total PCAM amount below a particular potential temperature level is conserved quantity under adiabatic conditions. The local PCAM amount satisfies the conservation law by considering it with the horizontal flux and the generation and dissipation associated with non-adiabatic heating. By using PCAM flux, we can not only quantitatively evaluate the cold air outflow, but also consider its balance. Therefore, PCAM flux anomalies explain the warm anomalies in East Asia and the NH mid-latitudes. In the zonal mean analysis, wave convergence and EDC show a balanced relationship. The EDC is generated to restore the geostrophic wind balance that is disrupted by wave convergence, and the driving force for the EDC is mainly baroclinic wave activity in the isentropic perspective (Townsend and Johnson 1985; Iwasaki 1990, 1992). This study describes the characteristics of PCAM flux and EDC associated with record warm condition over East Asia in DJF 2019/2020, and describes the relationship with wave activity anomalies.

2. Data and methods

We used the Japanese 55-year reanalysis (JRA-55; Kobayashi et al. 2015) at 1.25° × 1.25° spatial resolution, 37 pressure levels (i.e., 1000 to 1 hPa) vertical resolution, and 6-hourly temporal resolution from 1958 to 2020; we also used 2-m air temperature based on JRA-55. Climatological normals were based on 1981–2010 data. Standard deviations for normalization of the anomalies were based on the interannual variability over 1981–2010.

To diagnose the PCAM stream, we used the PCAM analysis formulas derived by Iwasaki et al. (2014). PCAM amount and flux were calculated from the geopotential height, air temperature, zonal and meridional wind on mandatory pressure levels, surface pressure, surface (i.e., 10-m) zonal and meridional wind, and surface (i.e., 2-m) temperature. Following earlier studies using isentropic PCAM analysis (e.g., Iwasaki et al. 2014; Shoji et al. 2014; Kanno et al. 2015), the PCAM amount and flux were based on the air mass below the 280 K potential temperature. The mean meridional circulation and EP flux based on the MIM (Iwasaki 1989, 1992) method were analyzed to determine the relationship with surface temperature over Japan and the AO index. Here, we

Corresponding author: Chiaki Kobayashi, Meteorological Research Institute, 1-1 Nagamine, Tsukuba, Ibaraki, 305-0052, Japan. E-mail: ckobayas@mri-jma.go.jp.

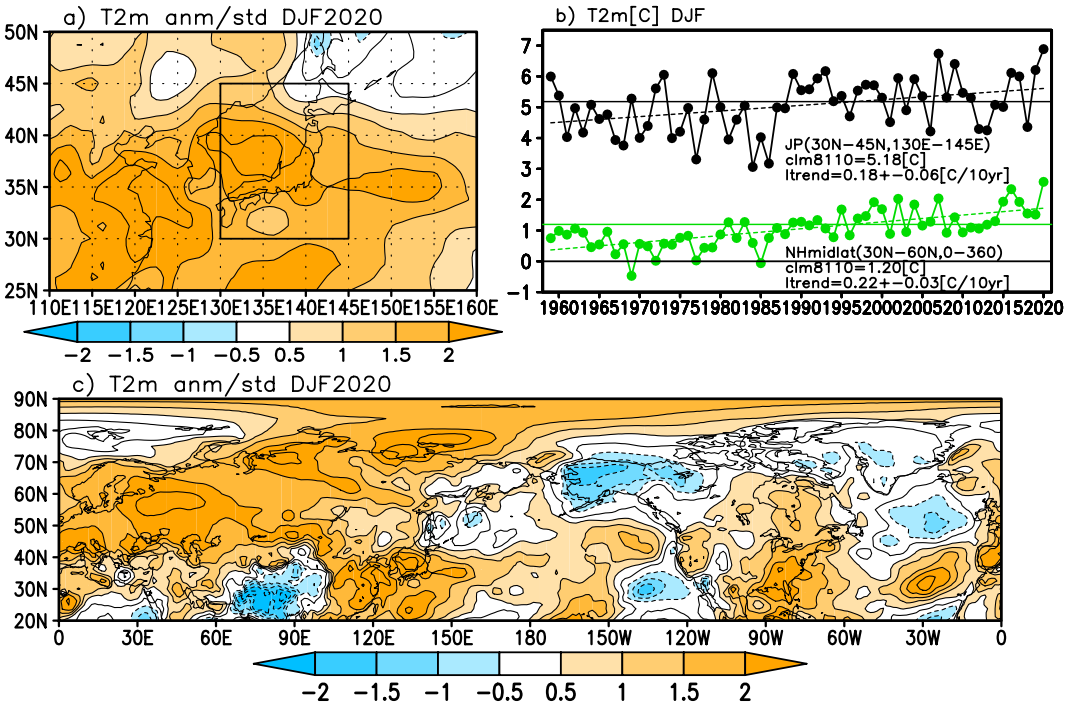

Fig. 1. (a) Seasonal mean 2-m air temperature anomalies over East Asia in DJF 2019/2020 normalized by standard deviations of DJF means based on JRA-55. (b) Interannual time series of DJF mean 2-m air temperature over Japan (130°E−145°E, 30°N−45°N; boxed area in (a)) and over the Northern Hemisphere (NH) mid-latitudes (0°−360°N, 30°N−60°N). Climate normals averaged from 1981 to 2010 and linear trend during the period from 1958/1959 to 2018/2019 are denoted in the panel. (c) Same as (a), but over the NH.

mainly focus on the seasonal mean DJF 2019/2020 features. For the AO index, we used the DJF mean of the NOAA Climate Prediction Center AO index (available at https://www.cpc.ncep.noaa.gov/products/precip/CWlink/daily_ao_index/ao.shtml).

3. DJF 2019/2020 conditions in the Northern Hemisphere mid-latitudes

3.1 Seasonal mean surface temperature

Figure 1a shows the seasonal mean surface temperature anomalies over East Asia in DJF 2019/2020, normalized by the standard deviations (σ) of DJF means. Surface temperature near East Asia exhibited positive anomalies of more than 1.5 σ during DJF; DJF surface temperature over Japan (130°E−145°E, 30°N−45°N; boxed area in Fig. 1a) was the highest since DJF 1958/1959 (Fig. 1b). Even with the linear trend subtracted, DJF temperature anomaly was positive by more than 1.5 σ; in the NH, positive temperature anomalies of more than 2.0 σ were observed over regions in China, the sea south of Japan, central Eurasia, and from Europe to the North Atlantic (Fig. 1c). The seasonal mean temperature over the NH mid-latitudes (i.e., 30°N−60°N) was the highest since DJF 1958/1959 (Fig. 1b) and also the highest in terms of anomalies after subtracting the linear trend.

3.2 Polar cold-air mass amount and flux

To diagnose the record-warm winter over East Asia, the spatial distributions of the PCAM amount and flux are displayed in Fig. 2. The PCAM amount over the mid- to high-latitudes of the Eurasian continent in DJF 2019/2020 was considerably smaller than the climatological seasonal mean (Figs. 2a and 2b), while the negative PCAM-anomaly areas correspond well with the positive temperature-anomaly areas in Fig. 1c. The PCAM flux intensity (Figs. 2c and 2d), which is the magnitude of the PCAM flux vector, was weaker than the climatological normal over the area from east coast of China to Japan. The intensity-anomaly pattern over East Asia indicates that the PCAM flux pathway shifted northeastward from the climatological position. The intensity-anomaly pattern over North America also shows that the PCAM flux was shifted northeastward from the climatological position.

Figure 3 shows the DJF meridional PCAM flux across 40°N. The southward (i.e., negative value) PCAM flux intensity in DJF 2019/2020 was the weakest near 120°E (i.e., near East Asia) since 1958/1959 (Fig. 3b), which was the western edge of the strong area in the climatological distribution (Fig. 3a). The zonally averaged southward PCAM flux across 40°N was also the weakest since DJF 1958/1959 (Fig. 3c). In DJF 2019/2020, the southward PCAM flux intensity was extremely small, not only over East Asia, but also over the entire NH.

To examine the relationship between surface temperature and the PCAM flux intensity over East Asia, a regression map of the PCAM flux on the seasonal mean surface temperature over Japan is shown in Fig. 4a. There is an area in East Asia near 40°N over which the PCAM flux intensity is strongly negatively correlated with surface temperature over Japan; areas with positive correlations are located north of the negatively correlated area. This spatial pattern corresponds well with the PCAM flux anomaly pattern in DJF 2019/2020 (Fig. 2d), indicating that the positive surface-temperature anomaly over Japan was related to the northeastward shift of the PCAM flux pathway over East Asia. The PCAM flux regression map on the detrended interannual variability of surface temperature over Japan (Fig. S1) shows a pattern similar to that shown in Fig. 4a. Thus, the PCAM flux in DJF 2019/2020 exhibits a pattern that tends to appear when East Asia has warm winter conditions. The Siberian high and the Japanese side of the Aleutian low were weak in DJF 2019/2020 (Fig. S2) and may have weakened the southward PCAM flux intensity over East Asia.

The regression map of the PCAM flux intensity on the AO index is shown in Fig. 4b. The AO index was strongly related to the PCAM flux pathway mainly at the North American side; strong positive correlation between the two is found in the area from the Labrador Peninsula to the North Atlantic Ocean, as noted by Kanno et al. (2017). This spatial pattern is similar to that of

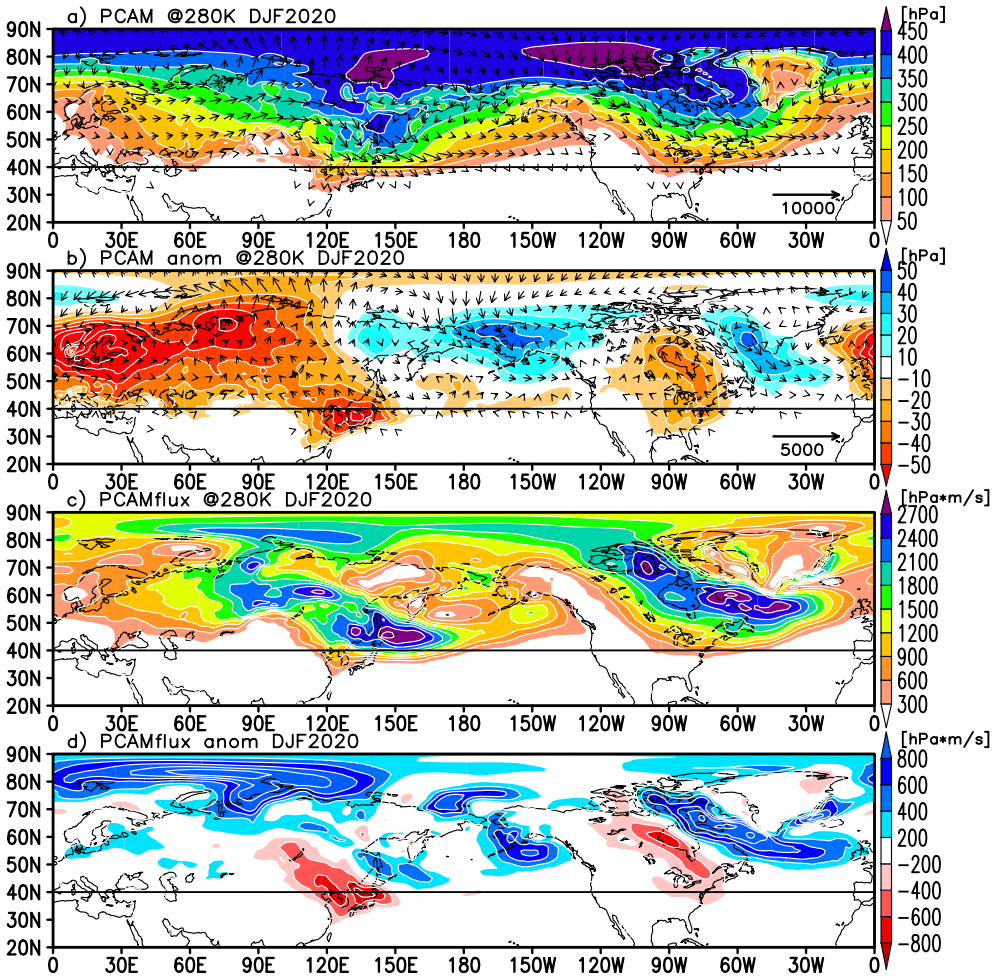

Fig. 2. (a) Seasonal mean polar cold-air mass (PCAM) amount below 280 K potential temperature (color) and PCAM flux (arrows) in DJF 2019/2020. (b) Same as (a), but for anomalies from climatology. (c) Same as (a), but for the intensity of the PCAM flux. (d) Same as (c), but for anomalies from climatology.

PCAM flux anomalies in the North American region during DJF 2019/2020, suggesting that the distribution of PCAM flux anomalies at the North American side is related to the AO. In East Asia, there is a region exhibiting moderate negative correlation between the PCAM flux anomalies and the AO index, which is consistent with the findings of Abdillah et al. (2017).

3.3 Zonal mean anomalies and extratropical direct meridional circulation

To display the characteristics of the northern hemispheric zonal mean fields in DJF 2019/2020, latitude–height cross sections of the anomalies of the EP flux divergence (EPFD), mass streamfunction, zonal mean temperature, and zonal mean zonal wind based on the MIM method, are shown in Fig. 5. Here, the vertical coordinate is the zonally averaged pressure on the isentropic surface (Iwasaki 1989). There are positive zonal mean temperature anomalies in the lower troposphere near 40°N; the zonal mean zonal wind exhibits easterly and westerly anomalies south and north of 40°N, respectively.

The EPFD anomaly is examined because the zonal mean zonal wind is affected by wave activity. The EPFD exhibited convergence anomaly at the mid-latitude (i.e., 30°N−40°N) lower troposphere (i.e., > 700 hPa) (Fig. 5a); conversely, at the mid-latitude (i.e., 40°N−60°N) upper troposphere (i.e., 400 hPa−250 hPa), the EPFD exhibited strong divergence anomaly. Both these anomalies indicate weaker wave–mean-flow interactions than climatological conditions (Fig. S3). In the upper troposphere, the EPFD anomaly balanced with weak EDC and the poleward heat transport is weakened accordingly. Due to the weak meridional heat exchange, the meridional temperature gradient is enhanced. It is consistent with the westerly wind anomaly, reflecting the thermal wind balance. This is consistent with the positive westerly wind anomaly observed at 40°N−60°N (Fig. 5d). Associated with the EPFD anomalies, the EP flux exhibited a downward anomaly in the mid-latitudes (Fig. 5a). As shown in Figs. 6c, 6e, and 6f, the EP flux-related variables over mid-latitudes in DJF 2019/2020 were the first and second extreme records since 1958/1959, respectively.

The EPFD is also related to the EDC, since it is almost in balance with the Coriolis force of the equatorward flow in the extratropics. Corresponding to the EPFD anomalies (Fig. 5a), the mass streamfunction shows a weak anomaly in the EDC (Fig. 5b). In 2019/2020, the mass streamfunction at 700 hPa and the southward wind at 850 hPa in the mid-latitudes exhibited the weakest values since 1958/1959 (Figs. 6b and 6d). As shown in Fig. S4, although the influence of the non-wave-driven component is not negligible in the climatological balance, the role of the non-wave-driven component is almost negligible in the lower meridional wind anomaly and EDC anomaly in DJF 2019/2020.

Iwasaki and Mochizuki (2012) indicated that the interannual variations of the mass streamfunction at 45°N and 850 hPa are positively (negatively) correlated with the zonal mean temperature in the lower troposphere north (south) of about 45°N, which is consistent with a simple thermodynamic consideration. The zonal mean temperature in DJF 2019/2020 exhibited positive anomaly in the mid-latitude lower troposphere (Fig. 5c), which is consistent with the weak EDC in winter. The relationship among the EP flux

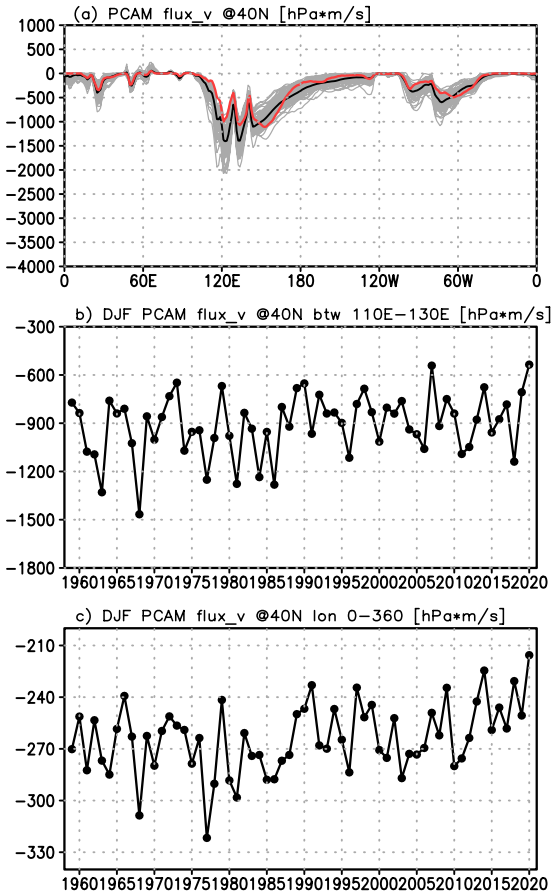

Fig. 3. (a) Meridional component of the DJF mean PCAM flux at 40°N in DJF 2019/2020 (red line), climatology (black line) and DJF seasons since 1958/1959 (gray lines). (b) Interannual variation of the meridional component of the PCAM flux between 110 and 130°E at 40°N. (c) Interannual variation of zonally averaged meridional PCAM flux across 40°N. The negative values indicate southward PCAM flux.

anomaly, meridional winds, and zonal mean temperature in winter can be explained by the relation shown in Iwasaki and Mochizuki (2012).

Although stationary ultra-long and transient long waves contribute to the formation of climatological EP flux convergence in the NH winter, interannual EPFD variations are mostly due to stationary waves (Kodama et al. 2010). The EPFD and EDC shown in Figs. 5a and 5b, which are averages of 6-hourly snapshots, are the sum of those of stationary and transient waves. To separate the EPFD and EDC into the contributions from steady and transient waves, we compute three-dimensional stationary fields of the global atmosphere by averaging temperature and wind over 1-month and evaluate the EPFD and EDC of stationary waves. The transient component is obtained by subtracting the stationary component from the total (Tanaka et al. 2004). Figures 5e–5h show the stationary- and transient-wave components of the EPFD and mass streamfunction anomalies in DJF 2019/2020. The EPFD and EDC anomaly patterns were mainly formed by the contribution of stationary waves; therefore, it is estimated that the EPFD and EDC anomalies in DJF 2019/2020 were mainly caused by the anomalous activity of stationary planetary waves.

4. Relation between PCAM flux and EDC

In this chapter, we confirm the statistical relationship between surface temperature over Japan and zonal mean field including meridional circulation. The zonal mean structures of the regression coefficient on the surface temperature over Japan and the AO index are shown in Fig. 7. The EDC variability was significantly negatively correlated with surface temperature in Japan (Fig. 7b), partly because the East Asia region is the main pathway for cold-air outflow over the NH during winter. As shown by Shoji et al. (2014), approximately 60% of the global southward PCAM flux at 45°N passes through the region over East Asia (90°E–180°E). The EPFD and the EDC anomaly patterns are mainly contributed by the stationary planetary wave anomaly (Figs. 7a and 7e).

The regression structures of the AO index (Figs. 7e–7h) are very similar to the anomaly patterns in DJF 2019/2020 (Figs. 5a–5d). The weak EDC anomaly associated with the weak upward EP flux near 45°N and positive anomalies of the zonal mean temperature near 40°N were observed in the regression structures, implying that the anomaly structures of the EDC and EPFD are linked to the positive AO phase. In addition, the regression structures of the EDC and EPFD on the surface temperature over

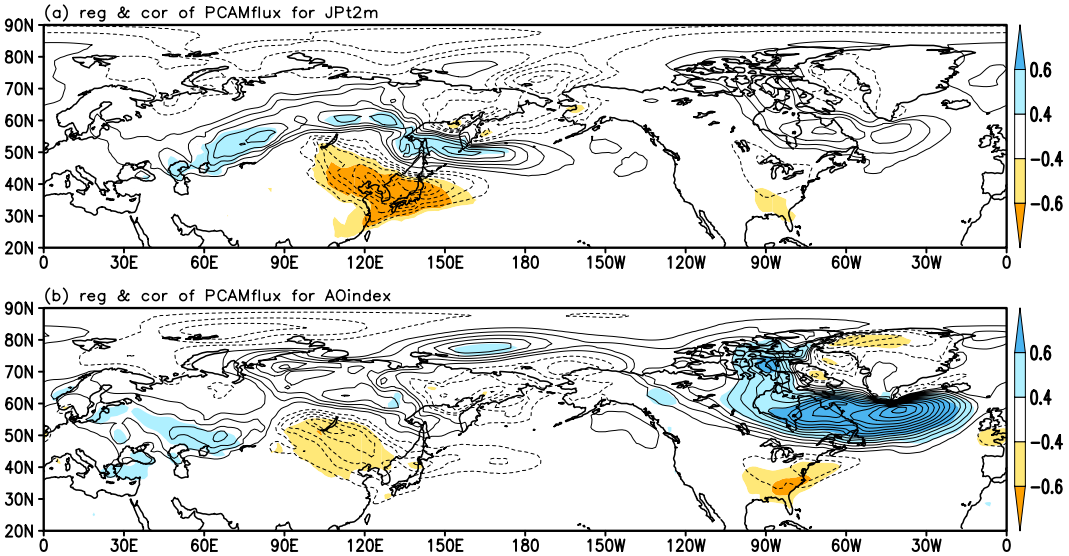

Fig. 4. (a) Regression (contour interval: 50 hPa · m/s) and correlation (shading) coefficient map for DJF mean PCAM flux on the 2-m air temperature over Japan (shown in Fig. 1b). Zero lines are not shown. (b) Same as (a), but for the AO index. Statistics were calculated for the 1959–2018 period.

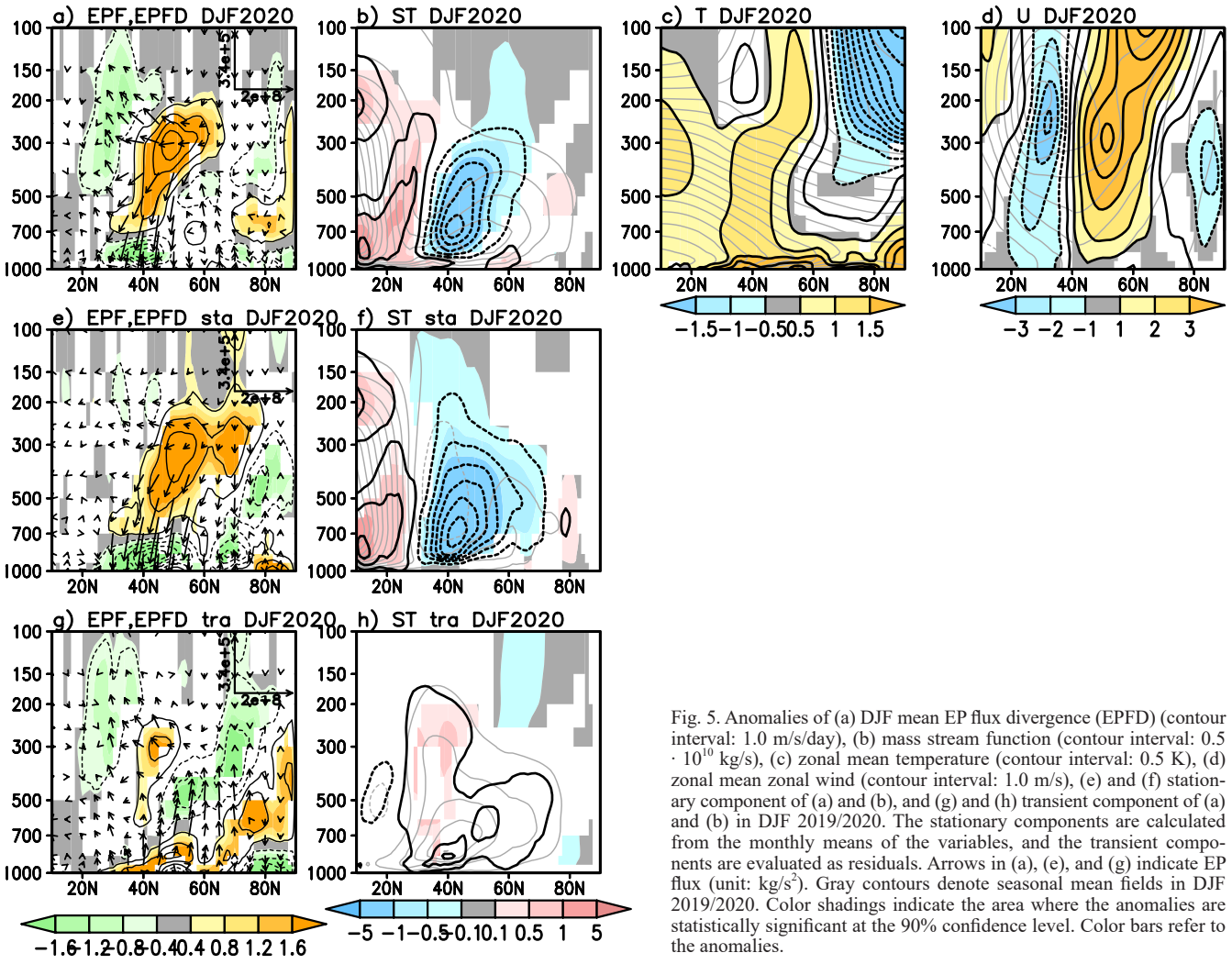

Fig. 5. Anomalies of (a) DJF mean EP flux divergence (EPFD) (contour interval: 1.0 m/s/day), (b) mass stream function (contour interval: 0.5 · 10^{10} kg/s), (c) zonal mean temperature (contour interval: 0.5 K), (d) zonal mean zonal wind (contour interval: 1.0 m/s), (e) and (f) stationary component of (a) and (b), and (g) and (h) transient component of (a) and (b) in DJF 2019/2020. The stationary components are calculated from the monthly means of the variables, and the transient components are evaluated as residuals. Arrows in (a), (e), and (g) indicate EP flux (unit: kg/s^2). Gray contours denote seasonal mean fields in DJF 2019/2020. Color shadings indicate the area where the anomalies are statistically significant at the 90% confidence level. Color bars refer to the anomalies.

Japan (Figs. 7a−7d) show a similar anomaly structure to those in DJF 2019/2020 (Figs. 5a−5d), especially in the lower troposphere, although the regression anomalies in the upper troposphere to the lower stratosphere are weak. This indicates that the formation of EDC anomalies in the lower troposphere is strongly linked to surface-temperature anomalies in Japan. Therefore, there is a possibility that the record-warm DJF 2019/2020 temperature over the NH mid-latitudes is related to the meridional circulation anomaly on a hemisphere scale. This consideration is consistent with Yu et al. (2015), who suggested that cold-air outflow at mid-latitudes is more robustly related to mass-circulation intensity at 60°N than to the AO index.

5. Summary

We examined the relationship between the record-warm winter (DJF) 2019/2020 over East Asia and the extremely weak circulation anomaly at a hemispheric scale. The Siberian high was weak in DJF 2019/2020, and the PCAM flux pathway shifted northeast and the PCAM flux was record weak in East Asia. We confirmed that this spatial pattern of PCAM flux anomalies tended to appear in warm winters in East Asia as a statistical relationship. In addition, the zonally averaged southward PCAM flux across 40°N was the lowest since DJF 1958/1959, related to weaker extratropical direct meridional circulation and weaker lower-level PCAM outflow over the NH mid-latitudes, which have resulted in warm winter conditions. Thus, the warm conditions in the NH mid-latitudes and East Asia during DJF 2019/2020 were presumably related to mean meridional circulation processes. The weak zonal mean circulation in DJF 2019/2020, mainly corresponding to weak stationary planetary wave activity, exhibited similar features to those seen during positive Arctic Oscillation (AO) phase; however, the relationship between the zonal mean fields and surface temperature over Japan was strong in the lower troposphere, indicating that the meridional circulation anomalies in the lower troposphere are closely linked to surface temperature anomalies over East Asia.

Further investigations focusing on the influence of teleconnections between these areas and the tropical oceans, which exhibited high surface temperature anomalies during the investigated period, will be necessary to clarify the causes of the modulation of stationary planetary waves in the lower troposphere. As noted by Kuramochi et al. (2021), the tripolar structure of anomalous convective heating was observed over the western tropical Indian Ocean, the Maritime Continent, and the central equatorial Pacific Ocean in DJF 2019/2020, resulting in heating and cooling of the atmosphere. The formation of anticyclonic circulation anomalies over East Asia as a result of this forcing might have been a factor regarding the warm winter in East Asia, as well as the modulation of stationary planetary waves, while it may have also affected the formation of positive AO through stratosphere-troposphere interactions.

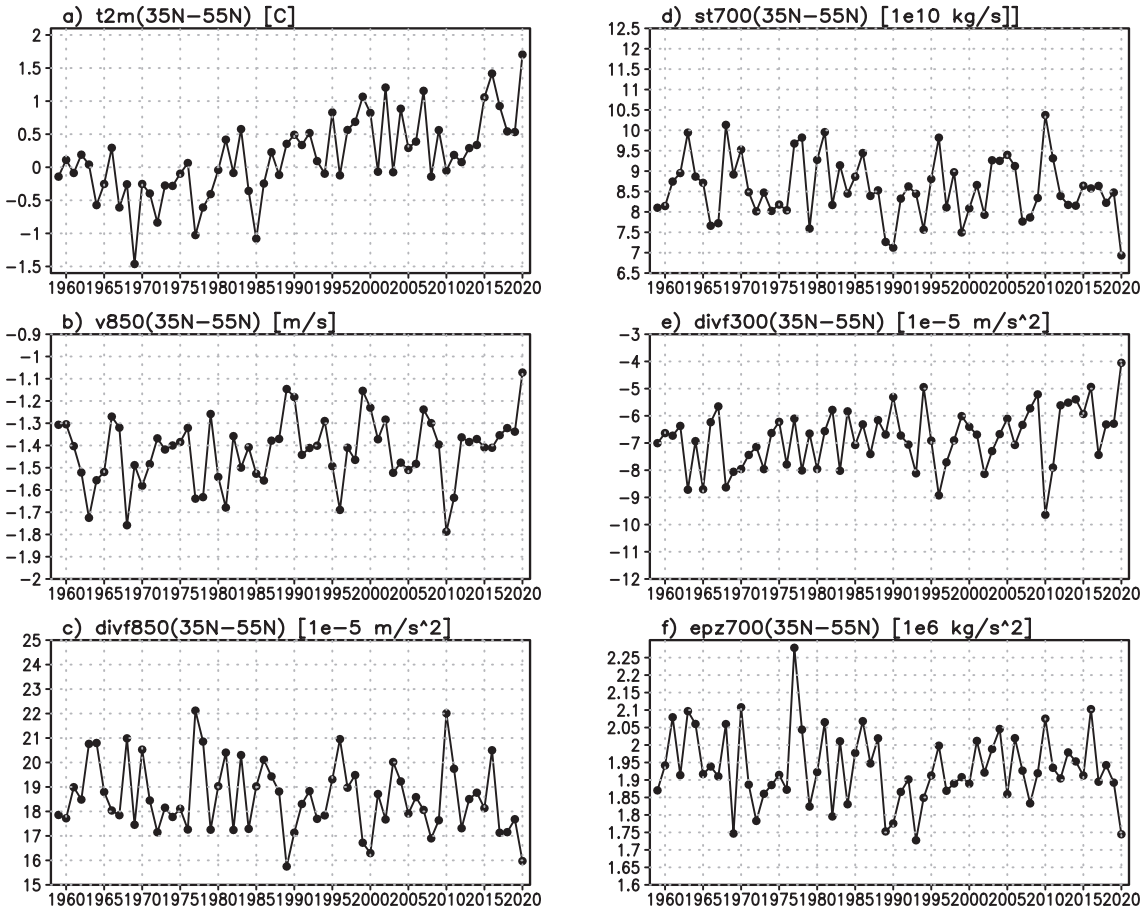

Fig. 6. Interannual time series of seasonal mean zonal mean (a) 2-m temperature (unit: C), (b) meridional wind at 850 hPa height (unit: m/s), c) EP flux divergence (EPFD) at 850 hPa height (unit: $1.0 \cdot 10^{-5}$ m/s^2), d) mass streamfunction at 700 hPa height (unit: $1.0 \cdot 10^{10}$ kg/s), (e) EPFD at 300 hPa height (unit: $1.0 \cdot 10^{-5}$ m/s^2), and (f) vertical component of EP flux at 700 hPa height (unit: $1.0 \cdot 10^{6}$ kg/s^2) over the area from 35 to 55°N.

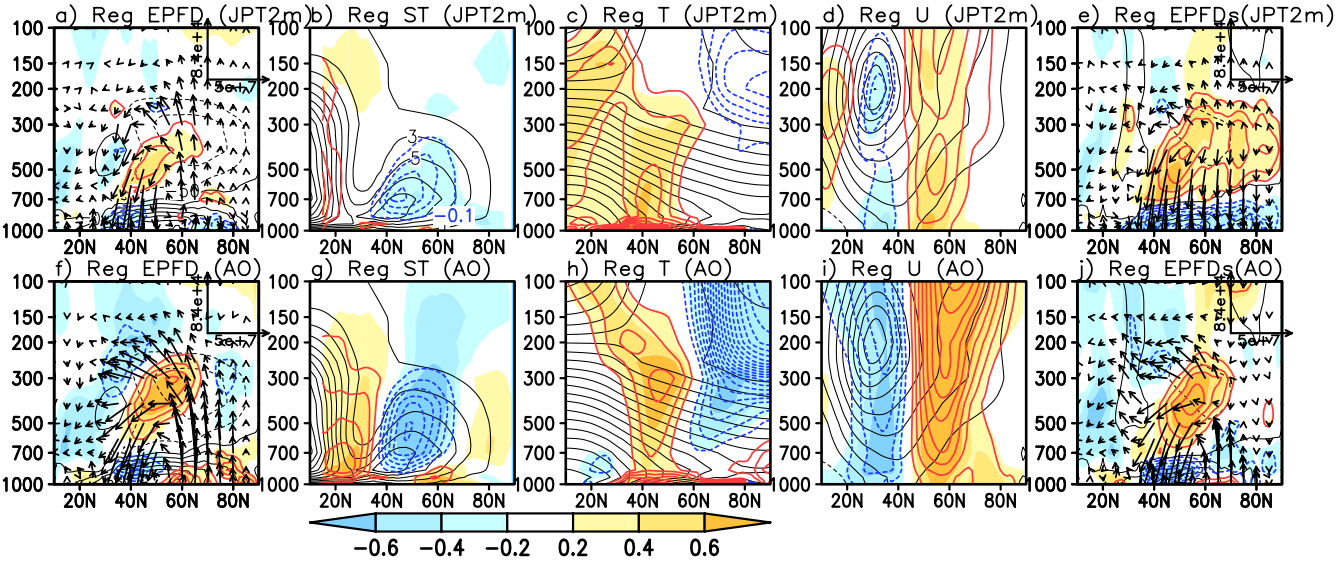

Fig. 7. Regression (red and blue contour) and correlation (shading) coefficient for DJF mean zonal mean fields on the 2-m air temperature over Japan (upper panels) and AO-index (lower panels) during the 1959–2018 period. Red and blue contour lines indicate positive and negative values, respectively. (a) (f) EP flux (arrows) and EPFD (contour interval: is 3 m^2/s^2); black contours show climatological mean of the divergence (contour interval: 50 m^2/s^2). (b) (g) Mass streamfunction (contour interval: $0.1 \cdot 10^{10}$ kg/s); black contours show climatological mean (contour interval is $2 \cdot 10^{10}$ kg/s). (c) (h) Zonal mean temperature (contour interval: 0.1 K); black contours show climatological mean (contour interval: 5 K). (d) (i) Zonal mean zonal wind (contour interval: 0.3 m/s); black contours show climatological mean (contour interval: 5 m/s). (e) (j) Same as (a) and (f), but for the stationary components.

Acknowledgements

This study was supported partly by the Japanese Ministry of Education, Culture, Sports, Science, and Technology (MEXT) KAKENHI Grant Number JP15H02129. YK is supported by MEXT KAKENHI Grant Numbers JP20H05167 and JP20H01976.

Edited by: R. Kawamura

Supplements

Figure S1 is the same as Fig. 4a, but on the detrended surface temperature over Japan. Figure S2 shows the seasonal mean sea-level pressure anomaly in DJF 2019/2020. Figure S3 is the same as Fig. 5, but for climatology. Figure S4 shows the wave-driven component of zonal mean meridional wind of MIM.

References

Abdillah, M. R., Y. Kanno, and T. Iwasaki, 2017: Tropical-extratropical interactions associated with East Asian cold air outbreaks. Part 1: Interannual variability. *J. Climate*, **30**, 2989−3007, doi:10.1175/jcli-d-16-0152.1.

Doi, T., S. K. Behera, and T. Yamagata, 2020: Predictability of the super IOD event in 2019 and its link with El Niño Modoki. *Geophys. Res. Lett.*, **47**, e2019GL086713, doi:10.1029/2019GL086713

Iwasaki, T., 1989: A diagnostic formulation for wave-mean flow interaction and Lagrangian-mean circulation with a hybrid vertical coordinate of pressure and isentropes. *J. Meteor. Soc. Japan*, **67**, 293−312.

Iwasaki, T., 1990: Lagrangian-mean circulation and wave-mean flow interactions of Eady's baroclinic instability waves. *J. Meteor. Soc. Japan*, **68**, 347−356.

Iwasaki, T., 1992: General circulation diagnosis in the pressure-isentrope hybrid vertical coordinate. *J. Meteor. Soc. Japan*, **70**, 673−687.

Iwasaki, T., and Y. Mochizuki, 2012: Mass-weighted isentropic zonal mean equatorward flow in the Northern Hemispheric winter. *SOLA*, **8**, 115−118.

Iwasaki, T., T. Shoji, Y. Kanno, M. Sawada, M. Ujiie, and K. Takaya, 2014: Isentropic analysis of polar cold airmass streams in the Northern Hemispheric winter. *J. Atmos. Sci.*, **71**, 2230−2243, doi:10.1175/JAS-D-13-058.1.

JMA, 2020: Climate characteristics of Japan's warmest-ever winter press release of Tokyo climate center (Available online at http://ds.data.jma.go.jp/tcc/tcc/news/press_20200501.pdf, accessed 7 Jul 2021).

Kanno, Y., M. R. Abdillah, and T. Iwasaki, 2015: Charge and discharge of polar cold air mass in Northern Hemispheric winter. *Geophys. Res. Lett.*, **42**, 7187−7193, doi:10.1002/2015gl065626.5.

Kanno, Y., J. E. Walsh, and T. Iwasaki, 2017: Interannual variability of the North American cold air stream and associated synoptic circulations. *J. Climate*, **30**, 9575−9590, doi:10.1175/JCLI-D-17-0104.1.

Kobayashi, S., and co-authors, 2015: The JRA-55 reanalysis: General specifications and basic characteristics. *J. Meteor. Soc. Japan*, **93**, 5−48, doi:10.2151/jmsj.2015-001.

Kodama, C., Y. Mochizuki, S. Hasegawa, T. Iwasaki, and M. Watanabe, 2010: Negative correlation between the interannual variabilities of the stationary and transient wave energy in the Northern Hemisphere. *SOLA*, **6**, 37−40, doi:10.2151/sola.2010-010.

Kuramochi, M., H. Ueda, C. Kobayashi, Y. Kamae, and K. Takaya, 2021: Anomalous warm winter 2019/2020 over East Asia associated with trans-basin Indo-Pacific connections. *SOLA*, **17B**, 9−13, doi:10.2151/sola.17B-001.

Lawrence, Z. D., J. Perlwitz, A. H. Butler, G. L. Manney, P. A. Newman, S. H. Lee, and E. R. Nash, 2020: The remarkably strong Arctic stratospheric polar vortex of winter 2020: Links to record-breaking Arctic Oscillation and ozone loss. *J. Geophys. Res. Atmos.*, **125**, e2020JD033271.

Shoji, T., Y. Kanno, T. Iwasaki, and K. Takaya, 2014: An isentropic analysis of the temporal evolution of East Asian cold air outbreaks. *J. Climate*, **27**, 9337−9348, doi:10.1175/JCLI-D-14-00307.1.

Tanaka, D., T. Iwasaki, S. Uno, M. Ujiie, and K. Miyazaki, 2004: Eliassen-Palm flux diagnosis based on isentropic representation. *J. Atmos. Sci.*, **61**, 2370−2383.

Townsend, R. D., and D. R. Johnson, 1985: A diagnostic study of the isentropic zonally averaged mass circulation during the First GARP Global Experiment. *J. Atmos. Sci.*, **42**, 1565−1579.

Yu, Y., R. Ren, and M. Cai, 2015: Comparison of the mass circulation and AO indices as indicators of cold air outbreaks in northern winter. *Geophys. Res. Lett.*, **42**, 2442−2448, doi:10.1002/2015GL063676.

Manuscript received 26 July 2021, accepted 8 November 2021
SOLA: *https://www.jstage.jst.go.jp/browse/sola/*